ORIGINAL PAPER

Dynamic Evolution and Identification of Bed Separation in Overburden During Coal Mining

Kaifang Fan[1,2] · Jianghui He[3] · Wenping Li[2] · Weichi Chen[2]

Abstract

Bed separation's evolution plays a crucial role in mining safety. Accurate identification of bed separation location is necessary to prevent disasters caused by bed separation. However, conventional methods such as theoretical calculation and in situ investigation cannot comprehensively reflect the dynamic evolution of the bed separation during mining. In this study, bed separations were classified as either supported or unsupported based on the stress state of the strata below a given bed separation. Furthermore, a theoretical method (PDLS-method) for identifying the dynamic location and aperture of bed separations during mining was proposed. In addition, in situ investigation was carried out to determine the internal movement of overlying strata and evolution law of bed separation. Monitoring results indicate that the internal movement of overlying strata has characteristics of "group movement" and "differential settlement". The rock layers in a strata group move synchronously, and adjacent strata groups move independently. Bed separations occur along the interfaces of those strata groups. The evolution of bed separation can be divided into four stages of emergence, rapid growth, stability, and recession. The biggest aperture of bed separation at investigation borehole was 1.56 m. The feasibility of the PDLS-method was verified by observed data. The results can be used in research regarding bed separation and prevention of secondary hazards.

Highlights

- A theoretical method for identifying the dynamic location and aperture of bed separations during mining was proposed.
- In-situ investigation was carried out to determine the internal movement of overlying strata and evolution law of bed separation.

- Internal movement of overlying strata caused by underground coal mining have characteristics of "group movement" and "differential settlement".

List of Symbols

E	Elasticity modulus
I	Moment of inertia
h	Thickness of the rock layer
h_m	Mining depth

✉ Jianghui He
hejianghui_aust@163.com

✉ Wenping Li
wenpingli516@cumt.edu.cn

Kaifang Fan
kaifangfan@163.com

Weichi Chen
weichichen159@163.com

[1] Department of Geotechnical Engineering, Nanjing Hydraulic Research Institute, Nanjing 210024, China

[2] School of Resources and Geosciences, China University of Mining and Technology, Xuzhou 221116, Jiangsu Province, China

[3] School of Earth and Environment, Anhui University of Science and Technology, Huainan 232001, China

h_s	Aperture of bed separation (calculated value)
h_{sf}	Aperture of bed separation (measured value)
$\overline{h_{sf}}$	Mean of measured value of aperture
H_0	Distance between the coal and rock layers
l	Length of the rock layer
l_{max}	Broken interval of the rock layer
L_m	Mining distance
M	Bending moment of beam
$[M]$	Ultimate bending moment
M_c	Mining thickness
q	Overburden load
Q	Shear force of beam
S_i	Free space under rock layer
k	Foundation coefficient
w	Deflection of beam
w_a	Settlement of the unsupported layer
w_s	Subsidence of the foundation
w_t	Settlement of the supported layer
$[\sigma]$	Tensile strength of the rock layer
θ	Rotation of beam
α	Feature coefficient
β	Caving angle
η	Bulking factor of the rock layer
γ	Density of the rock layer
$\varphi_1, \varphi_2, \varphi_3, \varphi_4$	Krylov functions
NS	Nash–Sutcliffe coefficient of efficiency
MAE	Mean absolute error

1 Introduction

Coal accounts for a large proportion of energy production and consumption, especially in China (Liu et al. 2018; Liu and Li 2019; Liu et al. 2019). Bed separation is a type of horizontal fracture caused by asynchronous settlement of adjacent overburden during coal mining (Peng 2006; Palchik 2003, 2005). Bed separation may act as a channel that can stores water (Fig. 1) and gas, which creates mining safety hazards and may result in severe casualties and/or property losses (Adhikary and Guo 2015; Fan et al. 2019; Gui and Lin 2016; Karacan et al. 2011; Palchik 2003, 2005). For example, on April 25, 2016, water inrush from a bed separation occurred in Zhaojin coal mine, China. The water inrush volume was greater than 32 thousand m^3, resulting in 11 deaths (Li et al. 2018). Separation layers are also primary injection locations for reducing mining-induced ground subsidence and deformation via grouting (Xuan and Xu 2014; Xuan et al. 2015; Sivakugan et al. 2006; Teng et al. 2016; Guo et al. 2019; Yang et al. 2019). Accurately predicting bed separation location and aperture during mining is necessary for the prevention of the secondary disasters caused by bed separation.

Bed separation is greatly influenced by rock properties, strata structures, and coal mining activities (Tadisetty et al. 2006; Wang et al. 2018; Yang et al. 2019), and its location, shape, size are paid extensive attention by international scholars and engineers. At present, research on bed separation is primarily focused on analyzing and predicting its occurrence and location through mechanical analysis (Yan et al. 2016;

Fig. 1 Schematic cross-section of engineering geological model of bed separation
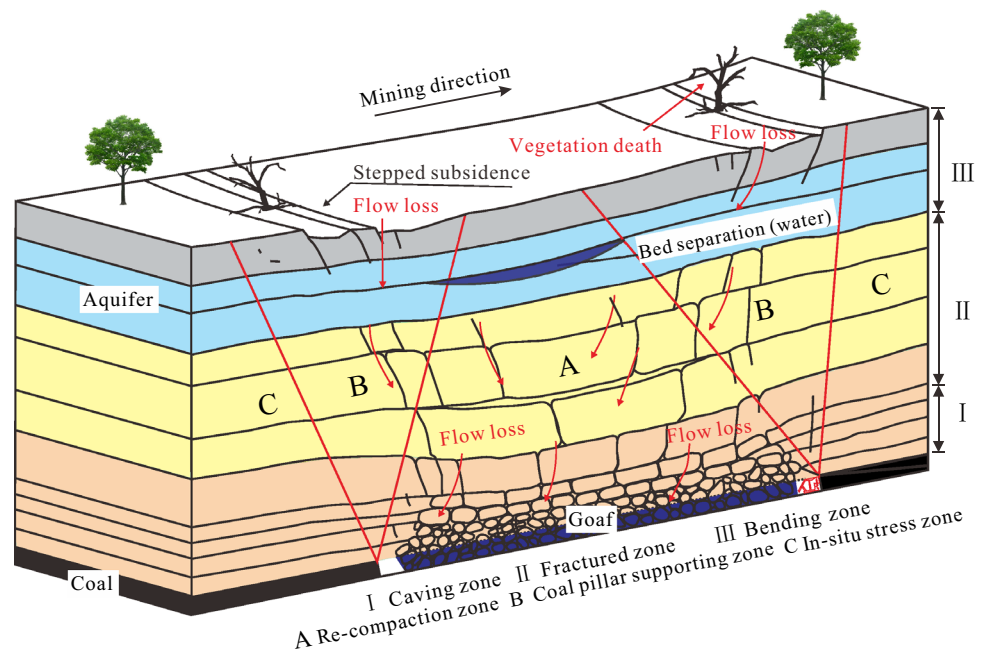
Gui et al. 2018), numerical simulation (Salmi et al. 2017; Xu et al. 2017; Yang et al. 2017), physical modeling (Ju and Xu 2013, 2015; Qin et al. 2021) and field monitoring (Karacan et al. 2014; Palchik 2010; Tan et al. 2013; Li et al. 2017a; Wang et al. 2021). According to field measurements results in Donetsk Coal Basin (Ukraine) in ten gas wells, Palchik (2003, 2005, 2010) correlated bed separation events with various mining activities and physical rock properties as well as established some empirical formulas. Using the geological penetration radar survey combined with borehole observations, Li et al. (2021) believed that an upright triangular collapsed pile masonry and an inverted triangular with larger fragments piled up alternately appear in the lower gob area. Gao (1996) considered that bed separation should be located above the fractured zone in the overburden, allowing each layer to deform and settle independently. The four-zone model has undergone significant progress in recent years (Cheng et al. 2017), however, the model only provides a qualitative analysis of the structural characteristics of roof overburden after strata subsidence, and the formation mechanism and evolution of bed separation were not considered. The impact of the overburden structure on strata behavior after mining has garnered the attention of some Chinese researchers. The 'key stratum theory' of Qian et al. (2003) considers that the entire or partial overburden movement after mining is controlled by strata structures of 'key stratum', and the distribution of bed separation is closely related to the structural characteristics of key stratum (Miao et al. 2011; Qian et al. 2003; Wang et al. 2017). Based on key stratum theory and composite beam theory, Yang et al. (1997) derived a theoretical formula for identifying bed separation locations by comparing the stiffness of adjacent strata from bottom to top, which has become a common theoretical basis for the study of bed separation location and bed separation related disasters in China (Gui et al. 2018; Miao et al. 2011; Yan et al. 2016). In the study of water inrush from separation layers, Fan et al. (2019) pointed out that the application scope was too narrow at Yang's method, and a modified Yang's method (MY-method) was given. Hou et al. (2020) suggested that the development characteristics of mining-induced strata fracture could be correctly predicted based on small amounts of observational data. Huang et al. (2018) suggested the maximum curvature of the stratum subsidence could be utilized to determine if the adjacent strata move independently or as a strata group. In addition, many researchers explained the phenomenon of separation layer by examining roof strata deformation and failure behavior (Huang et al. 2018; Meng et al. 2016; Rezaei et al. 2015; Wang et al. 2016; Yu et al. 2017) mining subsidence control (Xuan et al. 2015; Lian et al. 2020), natural gas drainage (Karacan et al. 2011), and other projects (Ju and Xu 2013, 2015; Karacan et al. 2014; Salmi et al. 2017; Wang et al. 2018).

Despite decades of studies, most predictive models still do not perform well in practical applications, especially when attempting to predict the dynamic location and aperture of bed separation during mining. The reason for this may be due to the very complicated bed separation physical mechanisms, which are still not fully understood. Field measurement of the dynamic development process of separation layer is very scarce, especially for deep seam mining. In addition, the associated temporal and spatial evolution of bed separation are not appropriately considered in the models of the current study.

Based on existing research results, first, a new theoretical method (PDLS-method) for identifying separation positions is proposed, which mainly includes two parts: determining potential separation positions before mining by MY-method, identifying the dynamic location and aperture of bed separations during mining. The method can account for temporal and spatial evolution of bed separation by introducing mining factors and considers geomechanics conditions. Finally, field measurement of the evolution of bed separation during longwall coal mining was carried out on the Yingpanhao mining area, and the PDLS-method was verified by the in situ measured data. The results are significant for mining subsidence control, methane drainage, and preventing water inrush from bed separation.

2 Identifying Potential Bed Separation Location

Under normal circumstances, the deformation of stiff and thick strata is generally small, while that of weak and thin strata is large (Xu et al. 2019; Wu et al. 2020). At the weak–strong rock layer interface, the interface is pulled apart if the tension on the interface is greater than the tensile strength of the interface itself (Yan et al. 2016), forming a void called bed separation (Fig. 1). As the interfaces between rock layers are weak structural planes, their tensile strength is nearly negligible compared to the weight of rock layers. Therefore, potential locations of bed separation could be identified by analyze and compare the
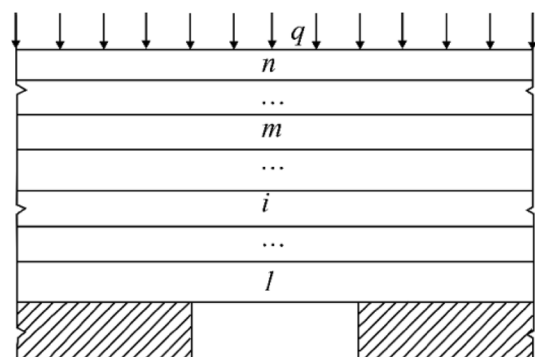

Fig. 2 Sketch showing the combined rock beam

structural and mechanical characteristics of the coal measure stratum.

As Fig. 2 illustrates, if there are n layers of strata above the goaf zone (from bottom up are coded as 1, 2,…, n), the elastic modulus, thickness, and density of each layer are E_i, h_i, and γ_i, then the load on stratum 1 can be derived as follows when considering a composite beam composed of n layers. Readers can refer to previous studies for deriving $(q_n)_1$ (Miao et al. 2011; Yan et al. 2016):

$$(q_n)_1 = \frac{E_1 h_1^3 (\gamma_1 h_1 + \gamma_2 h_2 + \cdots + \gamma_n h_n)}{E_1 h_1^3 + E_2 h_2^3 + \cdots + E_n h_n^3}. \tag{1}$$

According to modified Yang's method (MY-method), if $(q_m)_1 = \max((q_1)_1, (q_2)_1, \ldots, (q_n)_1)$, and $1 \leq m < n$, then potential bed separation occurs between the $m+1$th and mth layers; if $(q_n)_1 = \max((q_1)_1, (q_2)_1, \ldots, (q_n)_1)$, then potential bed separation does not occur between the 1st layer and nth layer (Fan et al. 2019).

The mechanical principles of MY-method can be interpreted as follows: if $(q_m)_1 = \max((q_1)_1, (q_2)_1, \ldots, (q_n)_1)$, and $1 \leq m < n$, then the 1st to mth layers can synchronously bend in the form of a rock group. In addition, $(q_m)_1 > \max((q_{m+1})_1, (q_{m+2})_1, \ldots, (q_n)_1))$, deformation of all strata between the $m+1$th and nth layers is less than that of the mth layer. Therefore, the interface between the mth and $m+1$th layers could be pulled apart by the mth layer.

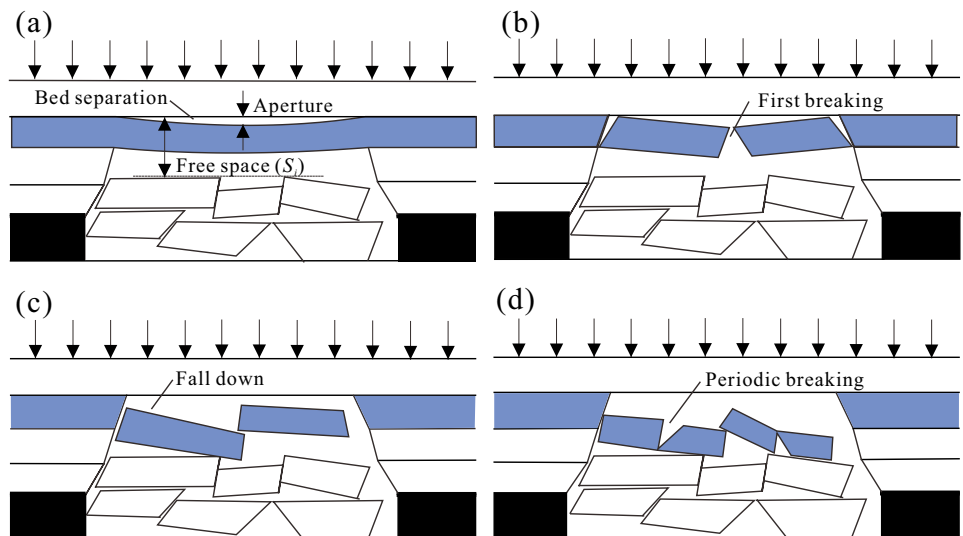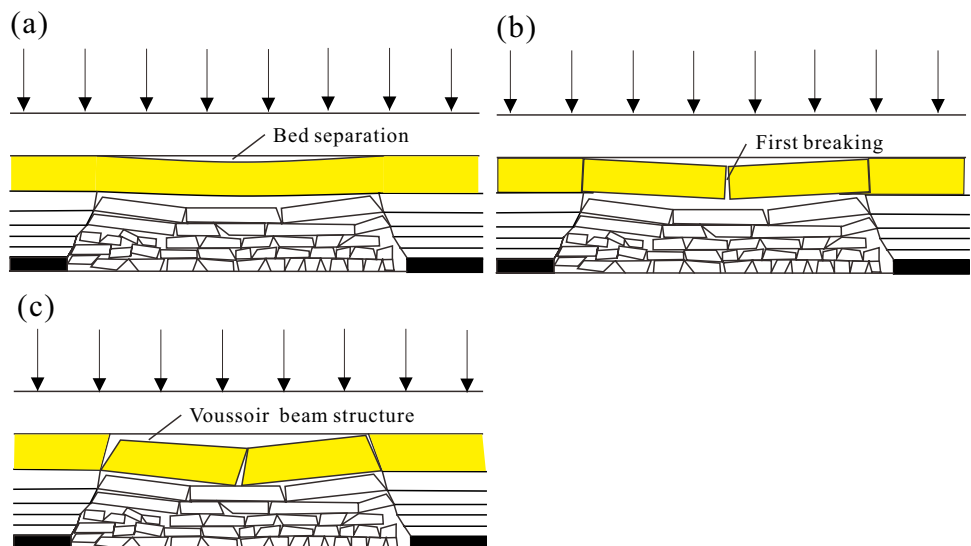Fig. 3 Breaking process of rock layer within caving zone

Fig. 4 Breaking process of rock strata within fractured zone

3 Dynamic Evolution Analysis of Bed Separation

3.1 Movement Characteristic of Rock Strata

After coal mining, a pressure balance arch can form in the overlying strata (Qin et al. 2021). The overburden weight outside of the pressure arch will be transmitted to the arch foot through the balance arch. Strata within the balance arch will bend under their own gravity. Specifically, in the caving zone, the fracture process of rock strata can be divided into four stages, just as Fig. 3 shows, i.e., the bed separation, first breaking, fall down and periodic breaking.

Due to the bulking of broken layer, the free space under rock layer diminishing with increasing height above coal floor. The free space under rock layer can be determined using the following equation (Ju and Xu 2015):

$$S_i = M_c - \sum_{j=1}^{i-1} h_j(\eta_j - 1), \tag{2}$$

where S_i is the free space, i.e., deformation and fall that rock layer is allowed, m; M_c is the mining thickness, m; η_j is the bulking factor on the jth layer stratum; and h_j is the thickness of the jth layer stratum, m.

Different free space under rock strata must result in different strata movement characteristics. In the fractured zone, after a small bed separation (Fig. 4a), first break of a rock layer occurs, while the fall of fractured rock layers does not occur due to the limit of space (Fig. 4b). After a small rotation, the broken rock block connects to each other and stops rotating after which the voussoir beam structure can be developed as Fig. 4c shows.

However, for the bending zone whose free space under rock layer is significantly smaller than those rock layer within the caving zone and fractured zone, thus the break of rock layer does not occur in bending zone due to the support of lower fractured rock mass. Hence, unlike those bed separations within the caving zone and fractured zone, in bending zone, the intact bed separation along weak-strong rock layer will not be destroyed by through-going vertical fractures, as shown in Fig. 1.

3.2 Classification of Bed Separation

Based on above analysis, bed separation can occur all zones of the mining-induced overburden, but its characteristics in three zones are different. In caving zone and fractured zone, the deformation and first break of strata groups below the
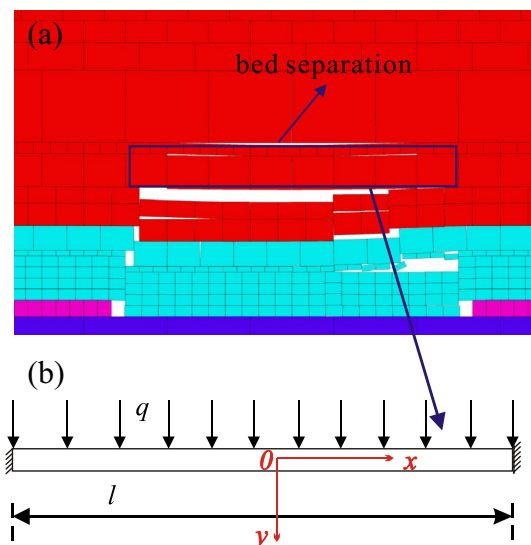

Fig. 5 Mechanical model for unsupported bed separation

separation layer are unaffected by the lower fractured rock mass in the goaf. The break of strata groups below the separation layer occurs rapidly along with the coal mining, the water-storage capacity of bed separation also quickly destroyed by through-going vertical fractures. Therefore, the possibility and extent of resulting bed separation water (gas) hazards are small (Gui et al. 2018). The bed separation within caving zone and fractured zone is not the focus of this article.

On the contrary, in bending zone, the bending of the strata group is limited by the fractured rock within the caving zone and fractured zone. Under the support of the collapsed rock mass, the rock group below the bed separation can be maintained for a long time without fracture, which leads to the large water-storage volume of bed separations in bending zone.

Hence, according to the stress state of the strata below a given bed separation, bed separation can be classified as two types: supported and unsupported.

Bed separation within the height of fractured zone is unsupported type (Fig. 5a). The lower and upper strata group in the cavity can be simplified as a uniformly loaded and fixed beam for mechanical analysis of deformation and first break, as shown in Fig. 5b.

Supported bed separation occurs outside the height of the fractured zone (Fig. 6). The upper strata group in the cavity can be simplified as a uniformly loaded and fixed beam for mechanical analysis. The lower strata group in the cavity
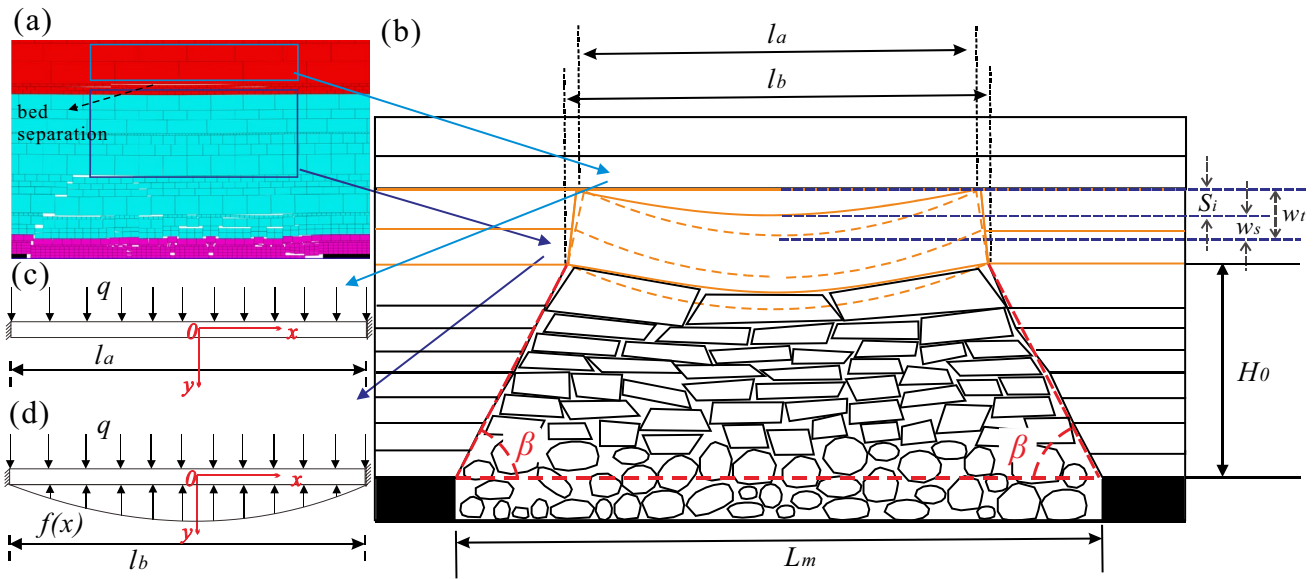
Fig. 6 Mechanical model for supported bed separation

can be simplified as the subsidence of fixed beam under supported condition.

3.3 Mechanical Models of Strata Group Around Bed Separation

According to material mechanics theory, the following equation is for deflection curve of fixed beam, and the broken interval l_{max} and deflection of can be calculated using the next following equations (Qian et al. 2003):

$$w(x) = \frac{qx}{24EI}\left(l^3 - 2lx^2 + x^3\right), \tag{3}$$

$$l_{max} = h\sqrt{\frac{2[\sigma]}{q}}, \tag{4}$$

$$w = \frac{ql^4}{384EI}, \tag{5}$$

where q is the accumulated load, which can be calculated using Eq. (1), kPa; EI is the bending stiffness, kN/m²; l is the length of the rock group, m; $[\sigma]$ is the tensile strength of the rock group, MPa; h is the thickness of the rock group, m.

As shown in Fig. 6b, final settlement of the lower strata group w_t consist of two factors. One is the free space before the strata group makes contact with the broken rock mass in the fractured zone, which can be determined using Eq. (2) (Ju and Xu 2015):

The other factor that determines settlement is the subsidence value after contact with the broken rock mass, denoted w_s, which can be calculated using the Winkler model (Winkler 1867):

$$f = kw_s b, \tag{6}$$

where k is the foundation coefficient, kN/m³; w_s is the subsidence of the foundation (i.e., deflection of the rock beam), m; b is the width of foundation beam, where $b = 1$ m in this paper.

Taking the center of rock beam as the origin, the x direction points along the advancing direction of the working panel, the positive y direction points vertically downward, and the unit length is taken along the z direction Fig. 6d. Considering the symmetry of the model, only the portion of the model where $x > 0$ is analyzed and calculated. The boundary conditions of the mechanical model are

$$\begin{cases} Q(x)_{x=0} = 0 \\ \theta(x)_{x=0} = \frac{dw_s(x)}{dx}\Big|_{x=0} = 0 \\ w_s(x)_{x=l/2} = 0 \\ \theta(x)_{x=l/2} = \frac{dw_s(x)}{dx}\Big|_{x=l/2} = 0 \end{cases} . \tag{7}$$

The differential equation and general solution for the deflected shape of the foundation beam are

$$EI\frac{d^4 w_s(x)}{dx^4} + kw_s = q, \tag{8}$$

$$w_s(x) = w_0\phi_1 + \theta_0\frac{\phi_2}{\alpha} - M_0\frac{\phi_3}{EI\alpha^2} - Q_0\frac{\phi_4}{EI\alpha^3}, \tag{9}$$

where $w0$, $\theta0$, $M0$, and $Q0$ are the deflection, rotation, bending moment, and shear force at $x = 0$, m, °, kN·m, kN, respectively. The parameters in Eq. (9) are defined as follows:

$$\begin{cases} \phi_1 = ch\alpha x \cos\alpha x \\ \phi_2 = \frac{1}{2}(ch\alpha x \sin\alpha x + sh\alpha x \cos\alpha x) \\ \phi_3 = \frac{1}{2}sh\alpha x \sin\alpha x \\ \phi_4 = \frac{1}{4}(ch\alpha x \sin\alpha x - sh\alpha x \cos\alpha x) \end{cases}, \tag{10}$$

$$\alpha = \sqrt[4]{\frac{k}{4EI}}. \tag{11}$$

As the upper part of the beam is subjected to a uniform load q, the deflection correction term is

$$w_{dc} = \frac{1}{\alpha^3 EI}\int_0^x q\phi_4[\alpha(x-\delta)]d\delta = \frac{q}{k}(1-\phi_1). \tag{12}$$

Then, the modified deflection equation is

$$w_s(x) = w_0\phi_1 + \theta_0\frac{\phi_2}{\alpha} - M_0\frac{\phi_3}{EI\alpha^2} - Q_0\frac{\phi_4}{EI\alpha^3} + \frac{q}{k}(1-\phi_1). \tag{13}$$

After calculation, the deflection and bending moment are as follows:

$$\begin{cases} w_s(x) = \frac{q}{k}\left[1 - \frac{\phi_2(l/2)\phi_1(x)}{\phi_1(l/2)\phi_2(l/2) + 4\phi_3(l/2)\phi_4(l/2)}\right] - \frac{q\phi_3(x)}{k\phi_3(l/2)}\left[1 - \frac{\phi_1(l/2)\phi_2(l/2)}{\phi_1(l/2)\phi_2(l/2) + 4\phi_3(l/2)\phi_4(l/2)}\right] \\ M(x) = -\frac{EIq}{k}\left[1 + \frac{4\alpha^2\phi_2(l/2)\phi_3(x)}{\phi_1(l/2)\phi_2(l/2) + 4\phi_3(l/2)\phi_4(l/2)}\right] + \frac{EIq\alpha^2\phi_1(x)}{k\phi_3(l/2)}\left[1 - \frac{\phi_1(l/2)\phi_2(l/2)}{\phi_1(l/2)\phi_2(l/2) + 4\phi_3(l/2)\phi_4(l/2)}\right] \end{cases}. \tag{14}$$

The maximum deflection of such a beam is at $x=0$ is

$$w_{s\,max} = \frac{q}{k}\left[1 - \frac{\phi_2(l/2)}{\phi_1(l/2)\phi_2(l/2) + 4\phi_3(l/2)\phi_4(l/2)}\right]. \tag{15}$$

The maximum bending moment of such a beam at $x=l/2$ is

$$M_{max} = -\frac{EIq}{k}\left[1 + \frac{4\alpha^2\phi_2(l/2)\phi_3(l/2)}{\phi_1(l/2)\phi_2(l/2) + 4\phi_3(l/2)\phi_4(l/2)}\right] \\ + \frac{EIq\alpha^2\phi_1(l/2)}{k\phi_3(l/2)}\left[1 - \frac{\phi_1(l/2)\phi_2(l/2)}{\phi_1(l/2)\phi_2(l/2) + 4\phi_3(l/2)\phi_4(l/2)}\right]. \tag{16}$$

When M_{max} reaches the ultimate bending moment $[M]$, the strata destroy at its mid-point, and the broken interval can be inversely calculated using $M_{max} = [M]$. Generally, $[M] = [\sigma]h^2/6$, where $[\sigma]$ is the tensile strength of rock group, MPa; and h is the thickness of rock group, m.

3.4 Prediction of Dynamic Evolution Characteristic of Bed Separation

According to the mechanical models for unsupported and supported layers, a new theoretical calculation approach for identifying the dynamic locations of bed separation (PDLS-method) is proposed.

First, the height of tensional stress-dominated zone (TSDZ) is determined according to mining distance, caving angle and mining depth. As the mining distance increases (Fig. 7), the shape of TSDZ changes from triangular to trapezoidal (Cheng et al. 2017). Therefore, the height of TSDZ (H_T) is
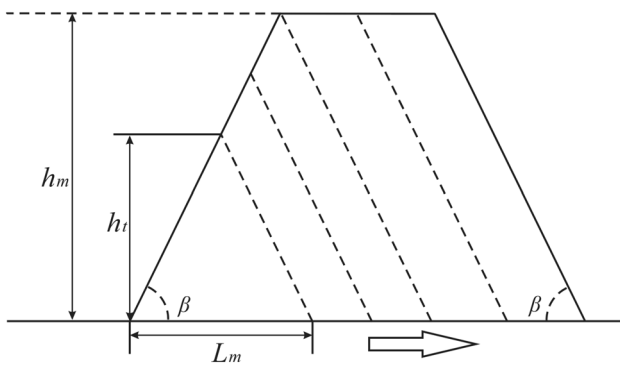
$$H_T = \min(h_m, h_t), \tag{17}$$
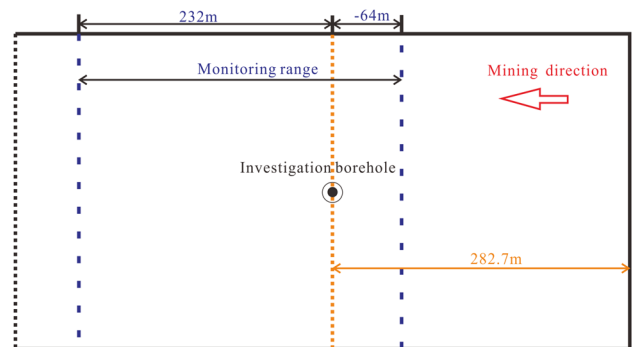

Fig. 7 Development of the TSDZ

Fig. 8 Schematic of investigation borehole location

where h_m is mining depth, m; $h_t = L_m \cdot (\tan\beta)/2$, L_m is mining distance, m; and β is the caving angle of the strata, °.

Second, the location of each bed separation in the TSDZ corresponding to different mining distances must be determined. The potential bed separation locations can be determined using the MY-method.
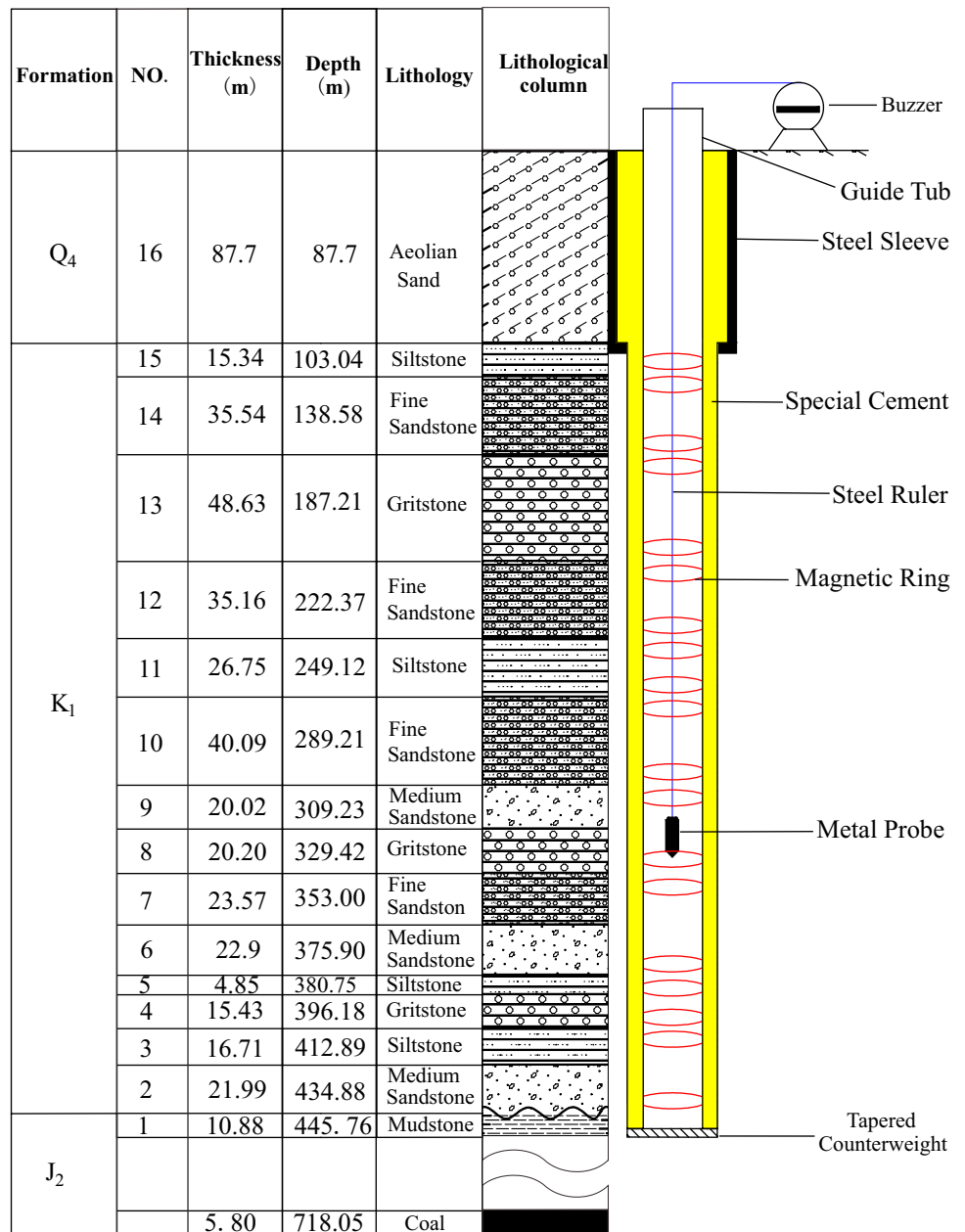
Finally, the distribution of a potential separation layer is determined based on physico–mechanical parameters and mining conditions. It is worth noting that the water(gas)-storage capacity of bed separation is destroyed when the separation layer is collapsed by vertical fractures or compacted by the upper rock strata. Given that the storage capacity is the base of the bed separation water (gas) hazard; therefore,

the intact bed separation exists when the following three criteria are satisfied simultaneously:

1. The limit span of rock layers above the separation layer is greater than its overhanging length, i.e., $l_{a\max} > l_a$;
2. The limit span of rock layers below the separation layer is greater than its overhanging length, i.e., $l_{b\max} > l_b$;
3. The aperture of bed separation, i.e., the difference in subsidence between the upper and lower strata of separation layer, is greater than 0, i.e., $h_s > 0$.

According to the geometric relationship for the collapsed overlying strata, the overhanging length of rock layers is as follows (Qian et al. 2003):

Fig. 9 Schematic of strata columnar section and steel ruler settlement instrument

Formation	NO.	Thickness (m)	Depth (m)	Lithology	Lithological column
Q$_4$	16	87.7	87.7	Aeolian Sand	
K$_1$	15	15.34	103.04	Siltstone	
	14	35.54	138.58	Fine Sandstone	
	13	48.63	187.21	Gritstone	
	12	35.16	222.37	Fine Sandstone	
	11	26.75	249.12	Siltstone	
	10	40.09	289.21	Fine Sandstone	
	9	20.02	309.23	Medium Sandstone	
	8	20.20	329.42	Gritstone	
	7	23.57	353.00	Fine Sandston	
	6	22.9	375.90	Medium Sandstone	
	5	4.85	380.75	Siltstone	
	4	15.43	396.18	Gritstone	
	3	16.71	412.89	Siltstone	
	2	21.99	434.88	Medium Sandstone	
J$_2$	1	10.88	445. 76	Mudstone	
		5. 80	718.05	Coal	

$$l = L_m - \frac{2H_0}{\tan\beta}, \tag{18}$$

where H_0 is the distance between the coal and rock layers, m.

The aperture of bed separation, i.e., the vertical distance between the upper and lower strata of separation layer, is

$$h_s(x) = w_t(x) - w_a(x). \tag{19}$$

In addition, the maximum aperture of bed separation is

$$h_s = w_t - w_a = \begin{cases} \dfrac{q_b l_b^4}{384 E_b I_b} - \dfrac{q_a l_a^4}{384 E_a I_a} & \text{when } \dfrac{q_a l_a^4}{384 E_a I_a} < S_i \\ S_i + \dfrac{q_b}{k}\left[1 - \dfrac{\phi_2(l_b/2)}{\phi_1(l_b/2)\phi_2(l_b/2) + 4\phi_3(l_b/2)\phi_4(l_b/2)} \right] - \dfrac{q_a l_a^4}{384 E_a I_a} & \text{when } \dfrac{q_a l_a^4}{384 E_a I_a} \geq S_i \end{cases}. \tag{20}$$

4 In Situ Investigation of Bed Separation

4.1 Geological Condition

The Yingpanhao mining area in the southwest of Dongsheng coalfield, located in Ordos, Inner Mongolia Autonomous Region, China, is a large modern coal mine with a production capacity of 12.0 Mt/a. The stratigraphic succession is composed of the Lower Jurassic Yan'an formation (J_{2y}), Middle Jurassic Zhiluo formation (J_{2z}), Middle Jurassic An'ding formation (J_{2a}), Lower Cretaceous Luohe formation (K_1l), and Quaternary (Q_4) (Fig. 9). The first coal seam to be mined is the 2–2 seam, with an average buried depth of 720 m and an average thickness of 6.41 m. The width of the longwall mining is 290 m. The geologic structure of the 2–2 seam and its overlying strata are simple with no fault and large folds, and the structures of the seam and overlying strata are near-horizontal.

The Luohe group is primarily composed of fine and medium sandstone. The rock is of an integral structure with relatively high mechanical strength. The bottom of the Luohe group is Jurassic An'ding group mudstone, which is sandy mudstone, and a water-resistant layer with relatively low strength. Longitudinally, this special combination of rock strata forms bed separations in the interface between the Luohe group and An'ding group in response to underground mining (Li et al. 2017b). Bed separations will accumulate water from the surrounding aquifer, constituting a hidden danger for safe mining.

4.2 Measurement Scheme

4.2.1 Investigation Borehole Structure

As shown in Fig. 8, one borehole was drilled from the ground of working panel 2202 before the 2–2 coal mining. The borehole was in the middle of the working panel, with distance of 282.7 m to the open-off cut. First, a borehole depth of 445.76 m was drilled from the ground, the
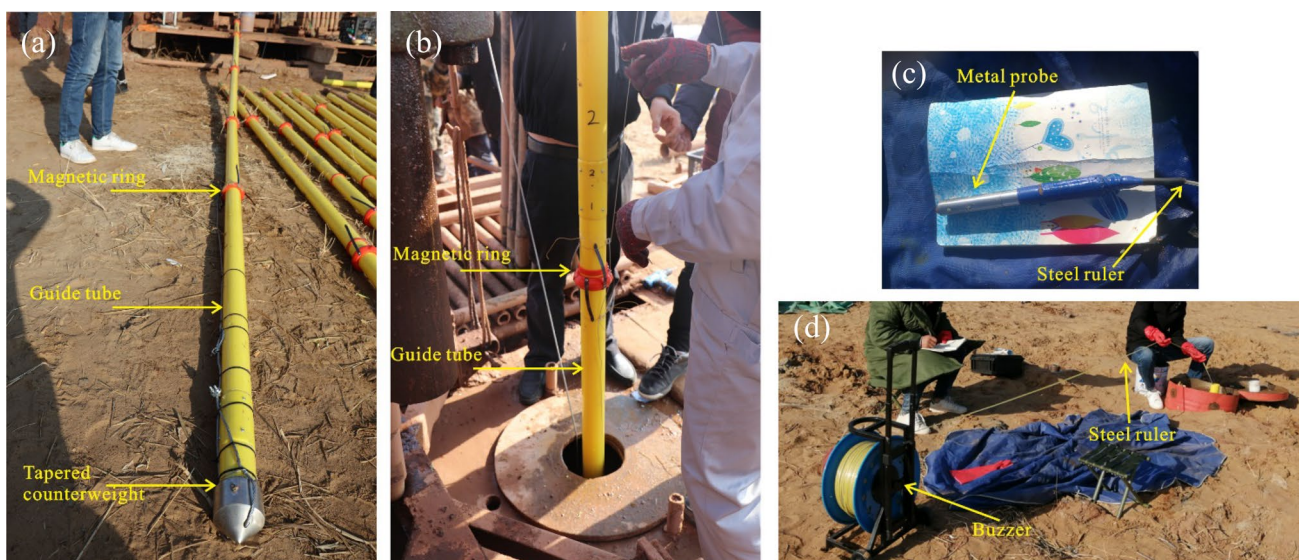

Fig. 10 Implantation and monitoring process of magnetic rings

Table 1 Initial measurements of magnetic rings buried depth

| No	Depth (m)	No	Depth (m)	No	Depth (m)	No	Depth (m)
1	90.65	16	204.29	31	317.82	46	413.36
2	96.89	17	213.18	32	323.53	47	416.42
3	106.54	18	222.02	33	329.67	48	419.38
4	114.50	19	231.13	34	338.48	49	422.27
5	124.81	20	239.93	35	347.46	50	426.34
6	135.81	21	248.90	36	356.52	51	429.25
7	140.57	22	258.04	37	365.45	52	431.22
8	150.43	23	263.96	38	374.47	53	432.33
9	159.44	24	269.83	39	377.44	54	436.78
10	168.87	25	272.96	40	389.50	55	438.06
11	174.37	26	278.77	41	398.43	56	440.07
12	180.23	27	287.89	42	401.38	57	441.51
13	185.48	28	291.74	43	404.35		
14	189.53	29	302.71	44	407.46		
15	195.15	30	308.85	45	410.37		
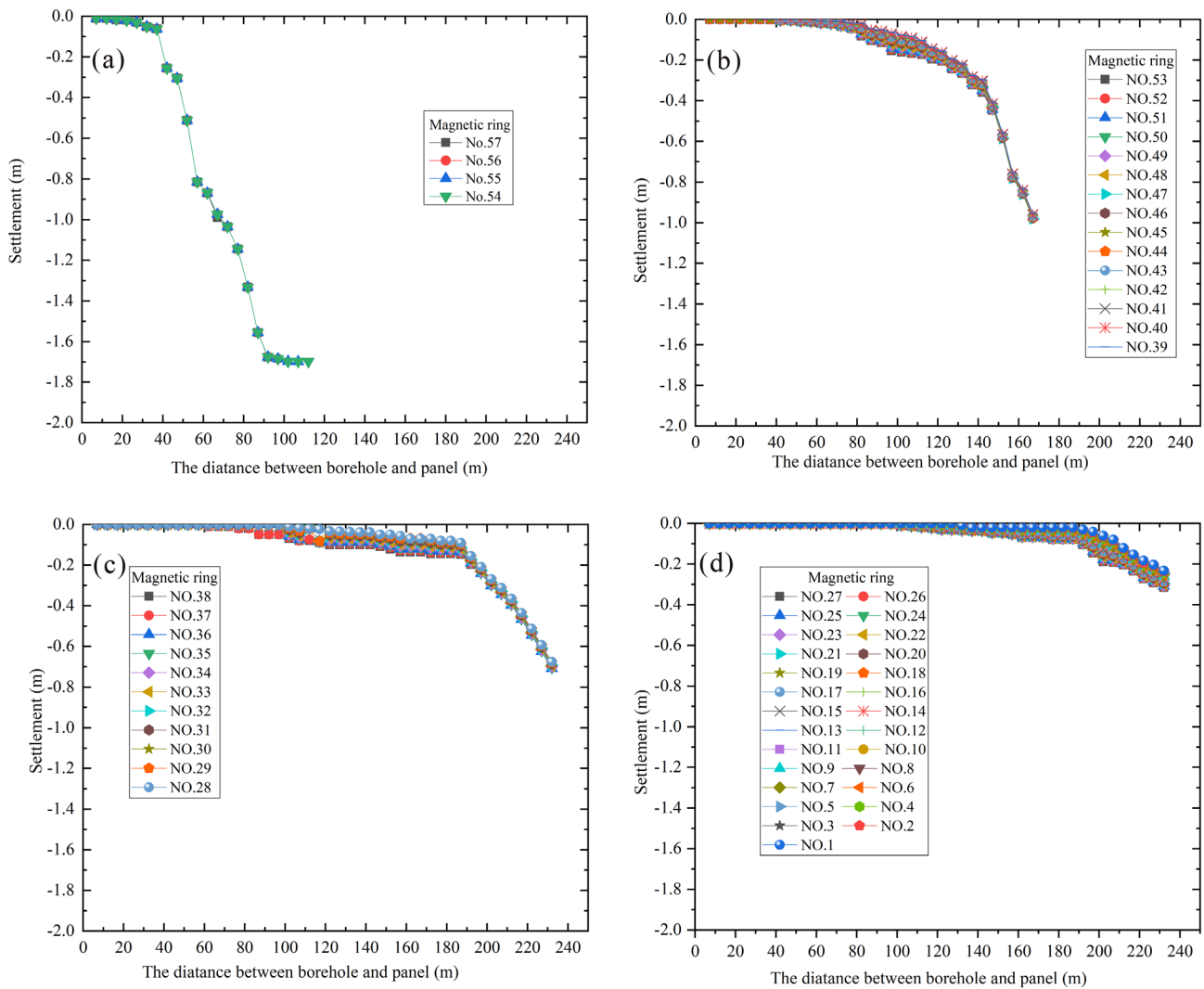
Fig. 11 Monitoring results of the settlement of magnetic rings inside overlying strata

diameter of borehole was 168 mm in unconsolidated layer and 150 mm in rock strata, and steel sleeve was implanted in unconsolidated layer (Fig. 9). Second, fixed the magnetic rings on the outside of the guide tube, and fixed the guide tube on the tapered counterweight before the embedding (Fig. 10a). Third, under the guidance of the tapered counterweight, the guide tube was gradually put into the borehole at a constant speed (Fig. 10b), and special cement was injected into the gap between the guide tube and the borehole. In addition, the buried depth of the coal seam was 718.05 m, and the mining thickness at the investigation borehole was 5.8 m (Fig. 9).

4.2.2 Observation of Layered Settlement

The observation instrument consists of buzzer, steel ruler, metal probe, guide tube and magnetic rings (Fig. 9). Put the metal probe in the investigation borehole through guide tube (Fig. 10c). The buzzer will output audio signal when the probe penetrated a magnetic ring, and meanwhile, record the value of steel ruler (Fig. 10d). Using this approach, the buried depth of magnetic rings during coal mining could be collected with a precision of 1 mm.

As shown in Fig. 8, the distance between investigation borehole and working panel marked as negative distance when the borehole is in front of the working panel, and the distance marked as positive distance when the working panel has passed the borehole. The monitoring frequency was 1–2 times per day, higher monitoring frequency occurred when the panel was closer to the monitoring borehole. The initial measurements of buried depths of magnetic rings were obtained (Table 1), when the distance between investigation borehole and working panel was − 64 m. A total of 56 groups of field data of 57 magnetic rings were collected, and the monitoring range was from − 64 to 232 m (Fig. 8).

4.3 Monitoring Results

The monitoring results show that the internal movement of overlying strata has characteristics of "group movement" and "differential settlement". As can be seen from Fig. 11, within the scope of monitoring, the overburden can divide into four strata groups: No. 57 to No. 54 magnetic rings (Fig. 11a), No. 53 to No. 39 magnetic rings (Fig. 11b), No. 38 to No. 28 magnetic rings (Fig. 11c), No. 27 to No. 1 magnetic rings (Fig. 11d). The rock layers in a strata group move synchronously, and adjacent strata groups move independently. Differential settlement, i.e., bed separations occur along the interfaces of those strata groups.

Furthermore, Fig. 12 illustrates the monitoring results of top and bottom magnetic rings of each strata group, i.e., the settlements of No. 57, No. 54, No. 53, No. 39, No. 38, No. 28, No. 27 and No. 1 magnetic rings. Magnetic rings settlement began when the panel passed the borehole. In the initial stage, the settlement of all magnetic rings was small, and there was no obvious differential settlement. With the advance of the panel, the differential settlement between No. 54 and No. 53 magnetic ring began to appear. After the panel passed borehole by 42 m, the subsidence of No. 54 magnetic ring increased significantly and finally becomes stable. When the working panel working panel had passed the borehole by 112 m, the borehole and guide tube were dislocated at the depth of about 433 m, and the settlement of No. 54 and lower magnetic rings could not be achieved by metal probe (Fig. 12b). As for No. 53 magnetic ring, the settlement began to slowly increase after a period of low settlement value. When the working panel passed through to 147 m beyond the borehole, the borehole and guide tube were broken again, and the testable depth of the investigation borehole was shortened to about 412 m. This indicates

Fig. 12 Monitoring results of dynamic evolution of bed separation
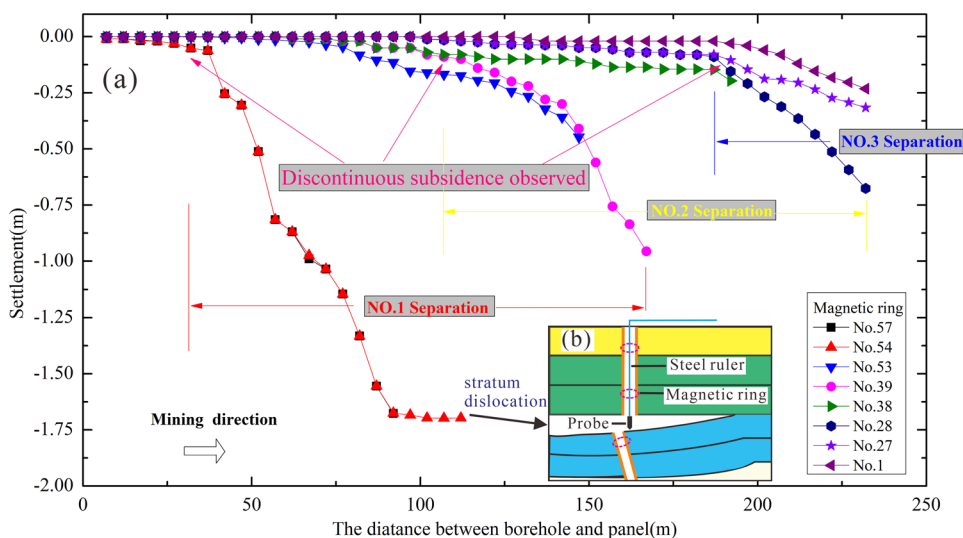
Table 2 Prediction and monitoring results of bed separation in 2202 mining panel

| No	Lithology	Thickness (m)	Depth (m)	Elastic modulus (GPa)	Tensile strength (MPa)	Monitoring results	MY-method
16	Aeolian sand	87.7	87.7				
15	Siltstone	15.34	103.04	6.5	1.65		
14	Fine sandstone	35.54	138.58	7.8	1.52		
13	Gritstone	48.63	187.21	3.3	1.44		
12	Fine sandstone	35.16	222.37	4.9	1.75		
11	Siltstone	26.75	249.12	6.5	1.08		
10	Fine sandstone	40.09	289.21	12.8	1.87	No. 3 bedseparation	No. 3 bed separation
9	Medium sandstone	20.02	309.23	4.4	1.35		
8	Gritstone	20.2	329.43	5.2	1.55		
7	Fine sandstone	23.57	353	6.6	1.7		
6	Medium sandstone	22.9	375.9	8.8	1.93	No. 2 bed separation	No. 2 bed separation
5	Siltstone	4.85	380.75	10.3	2.14		
4	Gritstone	15.43	396.18	6.5	1.66		
3	Siltstone	16.71	412.89	9.8	1.98		
2	Medium sandstone	21.99	434.88	7.1	2.45	No. 1 bed separation	No. 1 bed separation
1	Mudstone	10.88	445.76	5.2	2.11		

that the amount of rock stratum dislocation was close to or exceed the guide tube diameter (Fig. 12b).

The No. 39 magnetic ring was 54.89 m above No. 53 magnetic ring, and its settlement law was basically same as No. 53 magnetic ring. During coal mining, the differential settlement between No. 39 and No. 53 magnetic rings was tiny, which indicating that two magnetic rings belong to one moveable unit. At distance of about 167 m when the panel passed through borehole, the borehole and guide tube were dislocated at the depth of about 372 m.

No. 38 magnetic ring was 2.97 m above No. 39 magnetic ring. In the early stage of monitoring, the settlements of No. 38 and No. 39 magnetic rings were both tiny, and there were

basically synchronized. When the working panel advanced to 125 m beyond the investigation borehole, the differential settlement between two rings was increased steadily. When the working panel advanced to 192 m beyond the investigation borehole, the borehole and guide tube were broken, and the monitoring of No. 38 magnetic ring was terminated.

No. 28 magnetic ring was 82.7 m above No. 38 magnetic ring, and its settlement law was basically same as No. 38 magnetic ring. No. 27 magnetic ring was 3.85 m above No. 28 magnetic ring. At distance of about 232 m when the panel passed through borehole, the borehole was dislocated again, and the burial depths of all magnetic rings cannot be achieved by metal probe.

Fig. 13 Comparison between measured and calculation results at investigation borehole
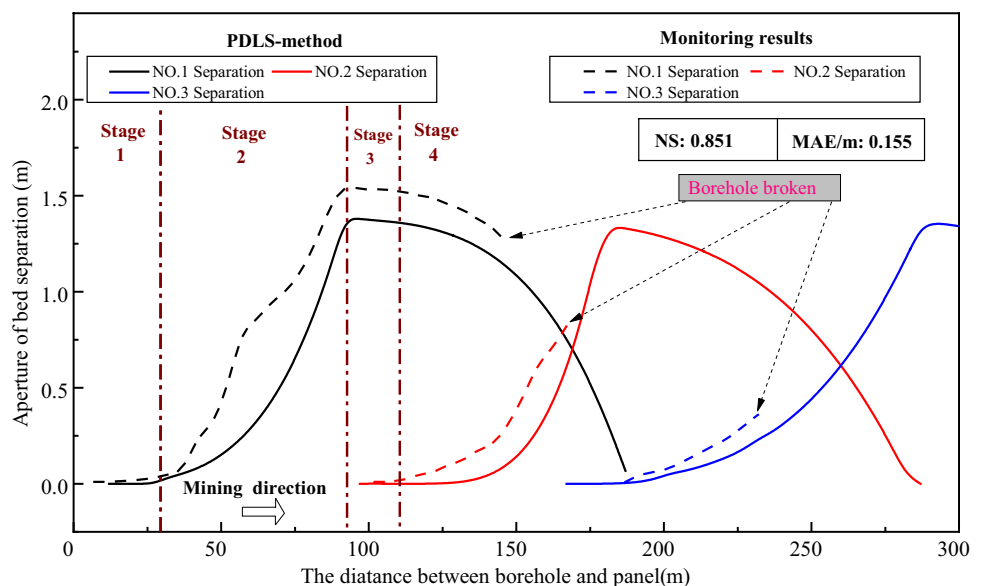
5 Comparison and Discussion

5.1 Validation of MY-Method

By the MY-method, the potential bed separation in the overlying strata of 2202 mining panel was predicted, the results were also listed in Table 2. To simplify the calculation, the density of each rock layer and unconsolidated layer were set to 24 and 14 kN/m³, respectively (Li et al. 2017a, b). The elastic modulus of the unconsolidated layers is much smaller than that of the rock mass; therefore, the loose layer can be reduced to a loading stratum using Eq. (1), and its elastic modulus is assumed to be 0 (Ju and Xu 2013). As shown in Table 2, the predicted results of the MY-method are consistent with the monitoring results, indicating that the MY-method is accurate.
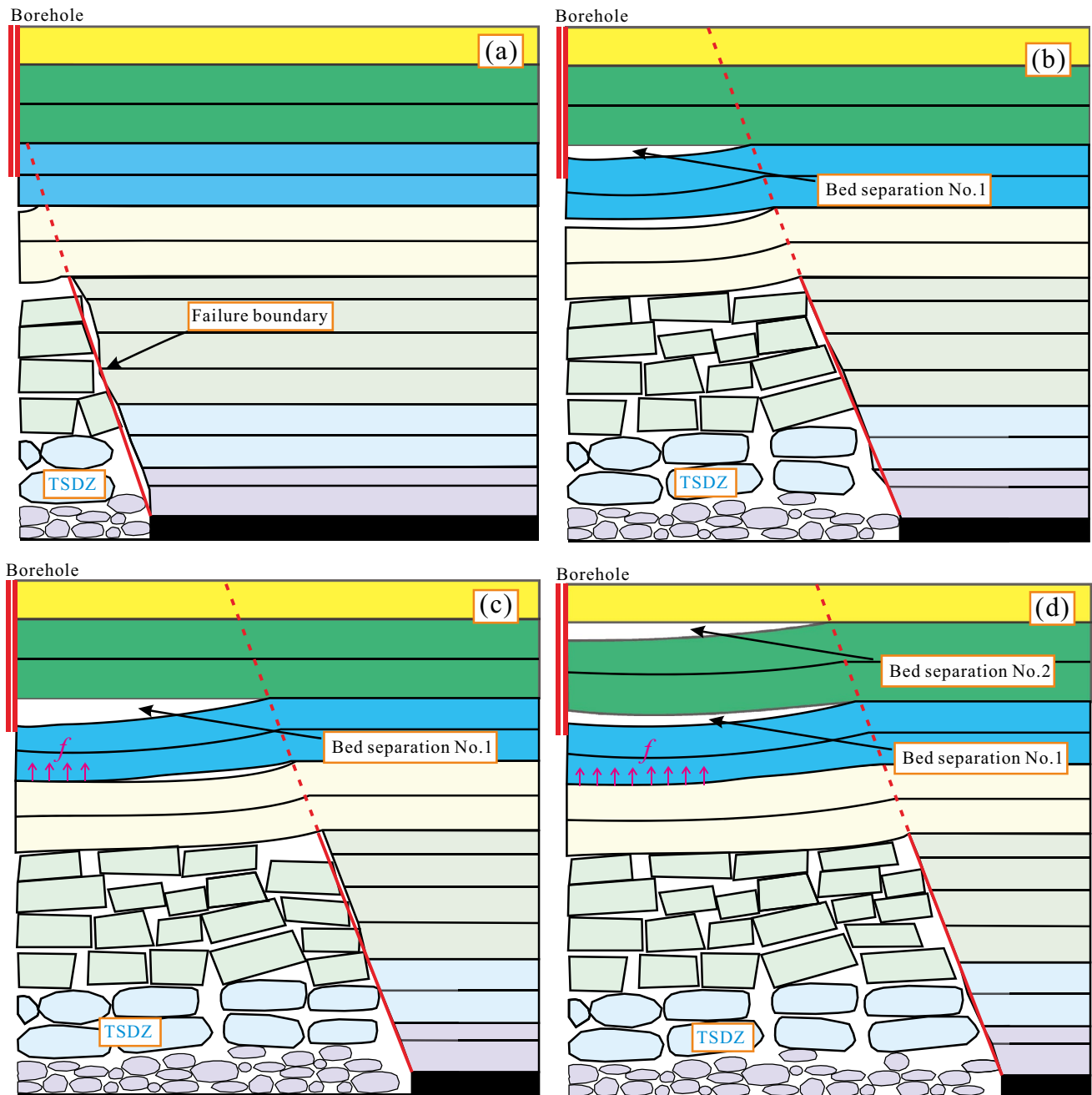

Fig. 14 Diagrams of dynamic evolution of bed separation

5.2 Validation of PDLS-Method

The aperture of each bed separation corresponding to different excavation lengths obtained using the PDLS-method and field measurement are shown in Fig. 13. The *x*-axis is the distance between borehole and panel, and the *y*-axis is the aperture of bed separation at investigation borehole, i.e., the vertical distance between the upper and lower strata in the separation layer. The error statistics of Nash–Sutcliffe (NS) coefficient of efficiency and mean absolute error (MAE) were calculated to evaluate the PDLS-method' accuracy and stability, which can be determined by the following equations, respectively (Chen et al. 2021):

$$NS = 1 - \frac{\sum_{i=1}^{n} \left| h_s - h_{sf} \right|_i^2}{\sum_{i=1}^{n} \left| h_{sf} - \overline{h_{sf}} \right|_i^2}, \tag{21}$$

$$MAE = \frac{1}{n} \sum_{i=1}^{n} \left| h_{sf} - h_s \right|_i, \tag{22}$$

where *n* is the measured number of targets; h_s is the calculated value of aperture, m; h_{sf} is the measured value of aperture, m; $\overline{h_{sf}}$ is the mean of measured value of aperture, m.

Due to the intense movement of overlying rock after coal mining, also limited by the monitoring means, the borehole and guide tube were dislocated many times during the monitoring period. Not whole development process of all bed separation was obtained. Among three bed separation, the monitoring data of No. 1 bed separation was relatively complete. As shown in Fig. 13, the development process of No. 1 bed separation can be divided into four stages of emergence, rapid growth, stability, and recession. The diagrams of No. 1 bed separation in each stage are shown in Fig. 14.

In the first stage, before the working panel had passed the borehole by 27 m (Fig. 13), the No. 1 bed separation had not occurred because the rock stratum still out of TSDZ (Fig. 14a). As the distance along the working panel increases, the scope of the TSDZ expands continuously, and the number of strata entering the TSDZ also increases gradually. In the second stage (Fig. 13), the lower strata group in No. 1 bed separation was sinking fast, and the void was rapid development (Fig. 14b). The biggest aperture of bed separation at investigation borehole was 1.56 m when the working panel had passed the borehole by 92 m. (Fig. 13). After rapid growth stage, the development process of No. 1 bed separation had entered a short period of stabilization. In this stage, the settlement of lower strata group in No. 1 bed separation was greatly limited by the lower rock mass, marked as *f* in Fig. 14c; however, the deformation of upper strata group in No. 1 bed separation was still small, thus the aperture of bed separation remained stable (Fig. 13). In the

fourth stage, after the working panel had passed the borehole by 112 m. (Fig. 13), the strata group above No. 1 bed separation begin sinking rapidly, the No. 1 bed separation began closing while that of No. 2 bed separation began to appear and expand rapidly (Fig. 14d). In general, the values of NS and MAS are 0.851 and 0.155 m, respectively (Fig. 13), which indicated that the PDLS-method was highly precision. The PDLS-method can be used to successfully predict the dynamic bed separation locations, and the four stages of the separation layer can be characterized by PDLS-method.

6 Conclusions

In this paper, dynamic evolution and identification of bed separation in overburden during coal mining was researched in detail based on theoretical calculation and in situ investigation. The main conclusions are summarized as follows.

1. Taking the height of the fractured zone as the boundary, a separation layer can be classified as unsupported or supported, depending on the stress state on the strata group below the separation layer. Supported bed separations above fractured zone can easily accumulate a large amount of water or gas, constituting a hidden danger for safe mining due to its large scale and long duration. It should be a focus of research into mining subsidence control, natural gas drainage, and preventing water inrush from bed separation.

2. A new theoretical approach (PDLS-method) that can be used to predict the dynamic location of a separation layer during longwall panel mining is introduced. Besides the overburden structure and mechanical properties, various mining factors, such as mining thickness, mining distance, mining depth, caving angle and bulking factor of strata, are also considered in PDLS-method.

3. The field investigation results indicate that the movement of overlying strata have characteristics of "group movement and differential settlement". The rock layers in a strata group move synchronously, and adjacent strata groups move independently. Bed separations occur along the interfaces of those strata groups. The evolution of bed separation can be divided into four stages of emergence, rapid growth, stability, and recession. The biggest aperture of bed separation at investigation borehole was 1.56 m when the working panel had passed the borehole by 92 m. The feasibility and rationality of PDLS-method were supported by with the in situ measured results.

It is an expensive, time-consuming and challenging task to onsite measuring the parameters of all bed separation within overlying strata. Using the theoretical mathematical

model to location the separation layer should be encouraged in further research; this is of great significance to safe mining.

References

Adhikary DP, Guo H (2015) Modelling of longwall mining-induced strata permeability change. Rock Mech Rock Eng 48:345–359

Chen W, Li W, Wang Q et al (2021) Evaluation of groundwater inflow into an iron mine surrounded by an imperfect grout curtain. Mine Water Environ 40:520–538

Cheng G, Ma T, Tang C et al (2017) A zoning model for coal mining-induced strata movement based on microseismic monitoring. Int J Rock Mech Min Sci 94:123–138

Fan K, Li W, Wang Q et al (2019) Formation mechanism and prediction method of water inrush from separated layers within coal seam mining: a case study in the Shilawusu mining area China. Eng Fail Anal 103:158–172

Gao YF (1996) "Four–zone" model of rock mass movement and back analysis of dynamic displacement. J China Coal Soc 21(1):51–55

Gui H, Lin M (2016) Types of water hazards in China coalmines and regional characteristics. Nat Hazards 84(2):1501–1512

Gui H, Lin M, Song X (2018) Identification and application of roof bed separation (water) in coal mines. Mine Water Environ 37(2):376–384

Guo W, Zhao G, Lou G et al (2019) A new method of predicting the height of the fractured water-conducting zone due to high-intensity longwall coal mining in China. Rock Mech Rock Eng 52:2789–2802

Hou E, Wen Q, Ye Z et al (2020) Height prediction of water-flowing fracture zone with a genetic-algorithm support-vector-machine method. Int J Coal Sci Technol 7:740–751

Huang WP, Li C, Zhang L et al (2018) In situ identification of water-permeable fractured zone in overlying composite strata. Int J Rock Mech Min Sci 105:85–97

Ju J, Xu J (2013) Structural characteristics of key strata and strata behaviour of a fully mechanized longwall face with 7.0 m height chocks. Int J Rock Mech Min Sci 58:46–54

Ju J, Xu J (2015) Surface stepped subsidence related to top-coal caving longwall mining of extremely thick coal seam under shallow cover. Int J Rock Mech Min Sci 78:27–35

Karacan CÖ, Olea RA (2014) Inference of strata separation and gas emission paths in longwall overburden using continuous wavelet transform of well logs and geostatistical simulation. J Appl Geophys 105:147–158

Karacan CÖ, Ruiz FA, Cotè M, Phipps S (2011) Coal mine methane: a review of capture and utilization practices with benefits to mining safety and to greenhouse gas reduction. Int J Coal Geol 86(2):121–156

Li S, Fan CJ, Luo MK et al (2017a) Structure and deformation measurements of shallow overburden during top coal caving longwall mining. Int J Min Sci Technol 27(6):1081–1085

Li D, Liu S, Zhang G et al (2017b) Typical roof water disasters and its prevention and control technology in the north of Ordos Basin. Int J Coal Geol 42(12):3249–3254

Li H, Chen Q, Shu Z et al (2018) On prevention and mechanism of bed separation water inrush for thick coal seams: a case study in China. Environ Earth Sci 77(22):759

Li Y, Ren Y, Peng SS et al (2021) Measurement of overburden failure zones in close-multiple coal seams mining. Int J Min Sci Technol 31:43–50

Lian X, Hu H, Li T et al (2020) Main geological and mining factors affecting ground cracks induced by underground coal mining in Shanxi Province China. Int J Coal Sci Technol 7:362–370

Liu SL, Li WP (2019) Indicators sensitivity analysis for environmental engineering geological patterns caused by underground coal mining with integrating variable weight theory and improved matter-element extension model. Sci Total Environ 686:606–618

Liu S, Li W, Wang Q (2018) Zoning method for environmental engineering geological patterns in underground coal mining areas. Sci Total Environ 634:1064–1076

Liu S, Li W, Qiao W et al (2019) Zoning method for mining-induced environmental engineering geological patterns considering the degree of influence of mining activities on phreatic aquifer. J Hydrol 579:124020

Meng Z, Shi X, Li G (2016) Deformation, failure and permeability of coal-bearing strata during longwall mining. Eng Geol 208:69–80

Miao XX, Cui XM, Wang JA, Xu JL (2011) The height of fractured water-conducting zone in undermined rock strata. Eng Geol 120(1):32–39

Palchik V (2003) Formation of fractured zones in overburden due to longwall mining. Environ Geol 44:28–38

Palchik V (2005) Localization of mining-induced horizontal fractures along rock layer interfaces in overburden: field measurements and prediction. Environ Geol 48:68–80

Palchik V (2010) Experimental investigation of apertures of mining-induced horizontal fractures. Int J Rock Mech Min Sci 47:502–508

Peng SS (2006) Longwall mining, 2nd edn. Science Press, Morgantown

Qian M, Shi P, Xu J (2003) Ground pressure and strata control. China University of Mining and Technology Press, Xuzhou

Qin Y, Xu N, Zhang Z et al (2021) Failure process of rock strata due to multi-seam coal mining: insights from physical modelling. Rock Mech Rock Eng 54:2219–2232

Rezaei M, Hossaini MF, Majdi A (2015) A time-independent energy model to determine the height of destressed zone above the mined panel in longwall coal mining. Tunn Undergr Space Technol 47:81–92

Salmi EF, Nazem M, Karakus M (2017) Numerical analysis of a large landslide induced by coal mining subsidence. Eng Geol 217:141–152

Sivakugan N, Rankine RM, Rankine KJ, Rankine KS (2006) Geotechnical considerations in mine backfilling in Australia. J Clean Prod 14(12):1168–1175

Tadisetty S, Matsui K, Shimada H, Gupta RN (2006) Real time analysis and forecasting of strata caving behaviour during longwall operations. Rock Mech Rock Eng 39:383–393

Tan Y, Yu F, Chen L (2013) A new approach for predicting bedding separation of roof strata in underground coalmines. Int J Rock Mech Min Sci 61:183–188

Teng H, Xu J, Xuan D et al (2016) Surface subsidence characteristics of grout injection into overburden: case study of Yuandian No. 2 coalmine China. Environ Earth Sci 75(6):1–11

Wang G, Wu M, Wang R et al (2016) Height of the mining-induced fractured zone above a coal face. Eng Geol 216:140–152

Wang S, Li X, Wang S (2017) Separation and fracturing in overlying strata disturbed by longwall mining in a mineral deposit seam. Eng Geol 226:257–266

Wang H, Xue S, Jiang Y et al (2018) Field investigation of a roof fall accident and large roadway deformation under geologically complex conditions in an underground coal mine. Rock Mech Rock Eng 51:1863–1883

Wang Z, Li W, Wang Q et al (2021) Monitoring the dynamic response of the overlying rock-soil composite structure to underground mining using BOTDR and FBG sensing technologies. Rock Mech Rock Eng 54:5095–5116

Winkler E (1867) Die lehre yon der elastizitat und festigkeit. H. Dominicus, Prague

Wu R, Kulatilake PHSW, Luo H et al (2020) Design of the key bearing layer and secondary mining technology for previously mined areas of small coal mines. Rock Mech Rock Eng 53:1685–1699

Xu N, Zhang J, Tian H et al (2017) Discrete element modeling of strata and surface movement induced by mining under open-pit final slope. Int J Rock Mech Min Sci 88:61–76

Xu C, Fu Q, Cui X et al (2019) Apparent-depth effects of the dynamic failure of thick hard rock strata on the underlying coal mass during underground mining. Rock Mech Rock Eng 52:1565–1576

Xuan DY, Xu JL (2014) Grout injection into bed separation to control surface subsidence during longwall mining under villages: case study of Liudian coal mine, China. Nat Hazards 73(2):883–906

Xuan D, Xu J, Wang B et al (2015) Borehole investigation of the effectiveness of grout injection technology on coal mine subsidence control. Rock Mech Rock Eng 48:2435–2445

Yan H, He F, Yan T (2016) The mechanism of bedding separation in roof strata overlying a roadway within a thick coal seam: a case study from the Pingshuo Coalfield China. Eng Fail Anal 62:75–92

Yang L, Yu G, Wang X et al (1997) Calculation of position of separated strata due to mining in coal mine. J China Coal Soc 22(5):477–480

Yang SQ, Chen M, Jing HW et al (2017) A case study on large deformation failure mechanism of deep soft rock roadway in Xin'An coal mine, China. Eng Geol 217:89–101

Yang X, Wen G, Dai L et al (2019) Ground subsidence and surface cracks evolution from shallow-buried close-distance multi-seam mining: a case study in bulianta coal mine. Rock Mech Rock Eng 52:2835–2852

Yu B, Zhao J, Xiao H (2017) Case study on overburden fracturing during longwall top coal caving using microseismic monitoring. Rock Mech Rock Eng 50:507–511

Publisher's Note Springer Nature remains neutral with regard to jurisdictional claims in published maps and institutional affiliations.